Journal of Nuclear Materials 403 (2010) 42–47

Contents lists available at ScienceDirect

Journal of Nuclear Materials

journal homepage: www.elsevier.com/locate/jnucmat

Effect of nano-SiC on the sintering behavior and properties of calcined carbon derived from mesocarbon microbeads

Hongyan Xia [a], Jiping Wang [a], Guiwu Liu [a,b], Zhongqi Shi [a], Guanjun Qiao [a,*]

[a] State Key Laboratory for Mechanical Behavior of Materials, Xi'an Jiaotong University, Xi'an 710049, China
[b] School of Aerospace, Xi'an Jiaotong University, Xi'an 710049, China

ARTICLE INFO

Article history:
Received 1 December 2009
Accepted 31 May 2010

ABSTRACT

Calcined carbon materials derived from mesocarbon microbeads (MCMBs) with or without pre-oxidative treatment were prepared and the effect of doped nano-SiC powder on the sintering behavior and properties was investigated. The results showed that the sintering shrinkage and density increment of the samples doped with 5 wt.% nano-SiC were higher than those with 3 wt.% and 10 wt.%, due to the amount of defects and extent of graphitization controlled by the content of nano-SiC. Physical and mechanical properties improved remarkably after doping a certain amount of nano-SiC. The highest bending strength of 122 MPa and lowest electric resistivity of 28 μΩ m were obtained when doping 5 wt.% nano-SiC in green MCMBs. Ball-milling contributed to reduction of particle sizes of MCMBs/nano-SiC mixtures and hence reduced or eliminated the gaps between particles in the calcined materials. The catalytic effect of nano-SiC can promote particle rearrangement and structure improvement during the sintering.

1. Introduction

Mesocarbon microbeads (MCMBs) have been used as an attractive precursor for high density and high strength carbon/graphite materials with moderate graphitizability [1,2]. They are adhesive carbonaceous grains extracted from mesophase pitch, and consist of aromatic oligomers where aromatic planes are stacked approximately parallel to each other in the same direction [3]. This special structure makes MCMBs have superior properties, such as self-sinterability, homogeneous shrinkage, high yield of carbon, and easy graphitization. At present, MCMBs are being studied and utilized in many different fields, including nuclear reactor walls, prosthetics, pistons for internal combustion engines, battery anodes, and seal materials [4–8].

Norfolk et al. [9,10] investigated the low-temperature sintering mechanism and high-temperature graphitization of MCMBs. The sintering involves two main stages: (i) neck formation between particles by a viscous phase non-densifying sintering mechanism (<527 °C) and (ii) rapid sample shrinkage due to crystallographic transformations (527–927 °C). In order to obtain suitable fusibility for adhesion during sintering, pre-oxidative stabilization of MCMBs was used to improve mechanical properties by inhibiting large voids, cracks, and deformed shape [11,12]. Wang et al. [2] reported that carbon discs from MCMBs with BP2000 (Black Pearls 2000), stabilized at 270 °C for 1 h and finally calcined at 1300 °C, showed the intimate adhesion among MCMBs particles with homogeneous texture, corresponding to their high compressive strength of 420 MPa. In addition, doping foreign materials into MCMBs can also improve the properties and extent of graphitization, or lower the heat treatment temperature of graphitization. Several research results revealed that some refractory-metal carbides (TiC, ZrC, VC and B_4C) and elements (B, Si, Ti and Zr) had the catalytic effect, resulting in the improvement of thermo-mechanical properties [13–16]. Moreover, Hu et al. [15] pointed out that Ti was the most effective catalyst among Ti, ZrO_2 and B_4C. And Liu et al. [16] further investigated the effect of Ti concentration on shrinkage and performance of MCMB-derived carbon laminations, and found that the electric resistivity increased and mechanical strength decreased when the Ti concentration was higher or lower than 7.5 wt.%.

However, relatively few prior studies exists on the effect of nano-SiC powder as dopant on the sintering and properties of MCMBs. Therefore, in this work we employed two systems of green MCMBs and pre-oxidative MCMBs to investigate the influence of nano-SiC concentration on sintering behavior and properties of the calcined MCMBs materials.

2. Experimental

2.1. Materials

Commercial MCMBs (Tianjin Tiecheng Battery Materials Co., Ltd., China) and nano-SiC powder (Hefei Kaier Nanometer Technology & Development Co., Ltd., China) were used as the starting materials. The mean particle size and maximum ash content of

* Corresponding author. Tel.: +86 29 82667942; fax: +86 29 82663453.
E-mail address: gjqiao@mail.xjtu.edu.cn (G. Qiao).

0022-3115/$ - see front matter © 2010 Elsevier B.V. All rights reserved.
doi:10.1016/j.jnucmat.2010.05.027

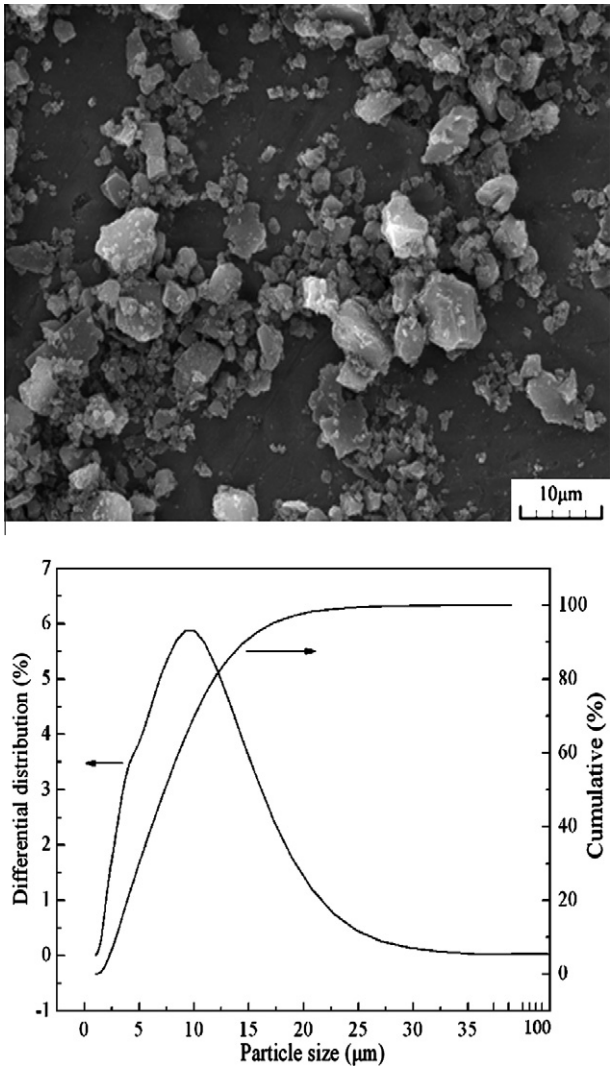

Fig. 1. SEM photograph and size distribution of the GMCMBs–5SiC mixture after ball-milling.

the MCMBs were ~21 μm (d_{10} = 15.1 μm, d_{50} = 21.1 μm and d_{90} = 29.5 μm) and 0.5 wt.%, respectively. The average size and purity of the nano-SiC powder were 40 nm and 99 wt.%, respectively.

2.2. Preparation

In order to investigate the effect of pre-oxidative stabilization on sintering and properties of the calcined carbon materials, before milling the MCMBs were divided into two parts: one was green MCMBs (GMCMBs) and the other was pre-oxidatively stabilized in air at 250 °C for 1 h (SMCMBs). In the following fabrication process, the nano-SiC powder was directly doped into the two MCMBs, and then ball-milling with agate balls in ethyl alcohol was applied in order to get homogeneous mixtures. The MCMBs–SiC mixtures after milling were molded uni-axially under 100 MPa for 30 s at room temperature to rectangular samples of 50 mm × 5 mm × 4 mm. At the same time, the pure MCMBs without dopant were directly molded to the rectangular samples. Sintering of all the samples was carried out at 1300 °C for 1 h in N_2 atmosphere at a heating rate of about 300–400 °C/h.

2.3. Characterization

The linear shrinkage rate of the sintered samples was determined geometrically by equation: $\Delta L/L_0 = 1 - L/L_0$, where ΔL, L_0 and L denote length variable, initial length and final length, respectively. The density increment was calculated by equation: $\Delta\rho/\rho_0 = \rho/\rho_0 - 1$, where $\Delta\rho$, ρ_0 and ρ denote density variable, initial density and final density, respectively. The bulk density ρ_b and open porosity P_{open} were examined by the Archimedes method defined by equations: $\rho_b = w_1/(w_2 - w_3)$ and $P_{open} = (w_2 - w_1)/(w_2 - w_3)$, where w_1, w_2 and w_3 denote the weight of the sample in air before soaking, the weights in air and distilled water after soaking (soaked in boiling distilled water for at least 2 h), respectively. Here the total porosity P_{total} was calculated by Eqs. (1) and (2) (the density of each component is 1.99 g/cm^3 for calcined carbon and 3.22 g/cm^3 for nano-SiC powder [17]):

$$\rho_r = \frac{m_{sintering}}{\frac{m_M - (m - m_{sintering})}{1.99} + \frac{m_{SiC}}{3.22}} \quad (1)$$

$$P_{total} = 1 - \frac{\rho_b}{\rho_r} \quad (2)$$

where ρ_b and ρ_r were the bulk and real density of calcined carbon; m_M, m_{SiC} were the masses of MCMBs and nano-SiC powder in the starting materials; m and $m_{sintering}$ were the masses of the carbon preform and the calcined carbon sample, respectively.

The bending strength of sintered samples with sizes of 3 mm × 4 mm × 20 mm was tested by three-point bending method using

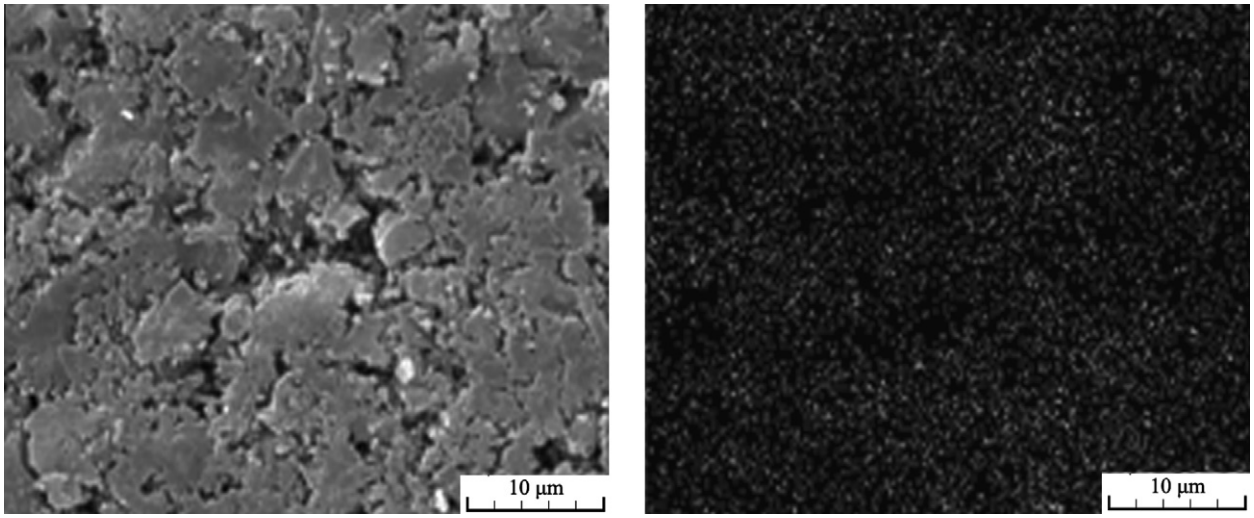

Fig. 2. SEM micrograph and Si elemental distribution map of the GMCMBs–5SiC green body.

an Instron-1195 testing machine. The loading speed was 0.5 mm/min. The electric resistivity was measured by the DC four-probe method and calculated by equation: $\lambda = [V/I] \times [hw/L]$, where V, I, L, h and w were the measured voltage, applied current, probe spacing, specimen thickness and width, respectively.

In order to clarify the microstructural change and elemental distribution of green compact or sintered samples after doping nano-SiC, the topographies of polished surfaces or cross-sections were characterized by scanning electron microscopy (SEM, VEGAII XMU, Tescan, Czech) coupled with energy dispersive spectroscopy (EDS, Model Oxford INCA, British). The size distribution of the green mixture after ball-milling was measured by a laser diffraction particle size distribution analyzer (Rise-2008, Jinan, China). Additionally, X-ray plate diffraction patterns (XRD, D8 Advance, Bruker, Germany) were obtained using a Cu Kα ($\lambda = 0.15406$ nm) monochromatized radiation source for determining the primary and parameter of the crystal lattice (d_{002}), indicating the extent of graphitization of calcined MCMBs.

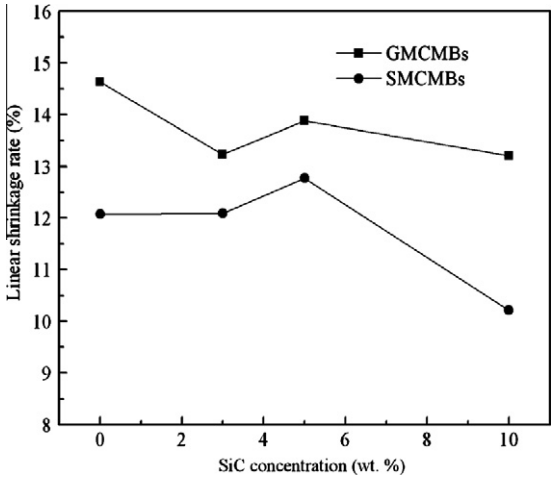

Fig. 3. Linear shrinkage rate of calcined carbon derived from GMCMBs and SMCMBs as a function of nano-SiC concentration.

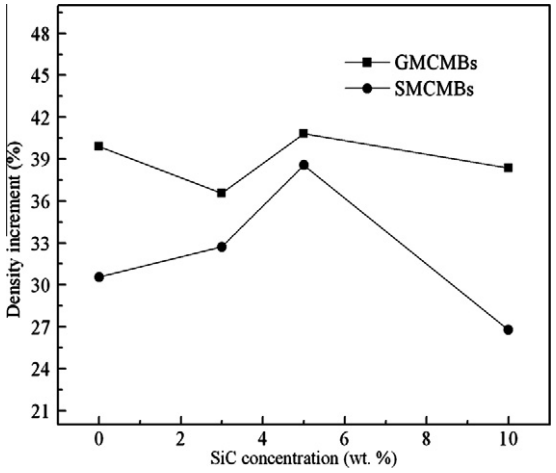

Fig. 4. Density increment rate of calcined carbon derived from GMCMBs and SMCMBs as a function of nano-SiC concentration.

3. Results and discussion

3.1. Green compact

After ball-milling, SEM photograph and size distribution of the GMCMBs–5SiC (with 5 wt.% nano-SiC) mixture is shown in Fig. 1. Morphological change and size reduction of the MCMBs can be seen clearly. The spherical particles were broken into smaller amorphous grains with a relatively large size distribution (d_{10} = 2.9 μm, d_{50} = 7.3 μm and d_{90} = 14.6 μm). The SEM micrograph and Si elemental distribution map of a green compact are also presented in Fig. 2. The Si element distributed uniformly, showing a homogeneous distribution of the mixed powders and no nano-SiC agglomerates after milling. However, some large pores existed on the surface of the green body, the reason might be that some large broken MCMBs inhibited the homogeneity during molding.

3.2. Sintering behavior

Fig. 3 shows the linear shrinkage rate of calcined carbon derived from GMCMBs and SMCMBs as a function of nano-SiC concentration (0, 3, 5, 10 wt.%). It can be seen that the linear shrinkage rate of SMCMBs–SiC system was lower than that of the GMCMBs–SiC system. The highest and lowest linear shrinkage rates, 14.6% and 10.2%, were obtained from the two sintered samples derived from GMCMBs–0SiC and SMCMBs–10SiC, respectively. Moreover, the two samples doped with 5 wt.% nano-SiC (i.e. GMCMBs–5SiC and SMCMBs–5SiC) had the highest linear shrinkage rate in their respective systems with SiC additions.

As mentioned in the section of introduction, the first step during sintering was the neck formation between particles by a viscous phase non-densifying sintering mechanism [9], so the content of viscous phase was a key factor to volume shrinkage. As we know, the higher the content of viscous phase in the green body, the more the amount of volatile matters, and thus the linear shrinkage rate will become higher. Therefore, the calcined carbon derived from GMCMBs–0SiC held the highest linear shrinkage rate because of the maximum content of viscous phase. Furthermore, the pre-oxidation process was performed in the SMCMBs system, some carbon and hydrogen were consumed by chemical reaction before sintering, resulting in the low content of viscous phase. As a result, the SMCMBs system had lower linear shrinkage rates than

Table 1
Physical and mechanical properties of calcined MCMBs with 0–10 wt.% nano-SiC.

Materials	Nano–SiC content (wt.%)	Bulk density ($g/cm^3 \pm 0.05$)	Open porosity (% ± 2.0)	Total porosity (% ± 2.0)	Electric resistivity (μΩ m ± 4)	Bending strength (MPa ± 10)
GMCMBs–0SiC	0	1.73	9.6	12.1	33	61
GMCMBs–3SiC	3	1.80	9.6	14.2	32	102
GMCMBs–5SiC	5	1.84	8.7	9.5	28	122
GMCMBs–10SiC	10	1.83	9.0	12.0	29	109
SMCMBs–0SiC	0	1.64	13.4	17.6	45	56
SMCMBs–3SiC	3	1.76	9.3	12.7	30	95
SMCMBs–5SiC	5	1.80	10.9	11.5	29	98
SMCMBs–10SiC	10	1.62	20.1	22.1	67	36

the GMCMBs system. In addition, doping nano-SiC into MCMBs can limit the volume shrinkage and improve the degree of graphitization of calcined carbon. According to the theory of catalytic graphitization of refractory-metal carbides on MCMBs [13], the nano-SiC particles within certain amount can contribute to sample shrinkage by improving the microstructure of carbon and accelerating crystallographic rearrangement. However, when the concentration of nano-SiC was over a certain value, much more defects were introduced into the samples and shrinkage limitation effect would play the main role. So it can be considered that the lowest linear shrinkage rate was resulted mainly from the large amount of defects induced by doping high content of nano-SiC. Therefore, the linear shrinkage rate of calcined carbon derived from MCMBs was mainly affected by the content of viscous phase, defect amount, and extent of graphitization controlled by the pro-oxidation process or the content of nano-SiC.

Fig. 4 shows the density increment rate of calcined carbon derived from GMCMBs and SMCMBs as a function of nano-SiC concentration. The change tendency of density increment rate was similar to that of the linear shrinkage rate and the reason was the same as described above. Similarly, the density increment rate of the GMCMBs–SiC system was higher than that of the SMCMBs–SiC system accordingly. The highest density increments of 40.8% and 38.6% were obtained for the two systems when doped with 5 wt.% nano-SiC, respectively.

3.3. Properties

The physical and mechanical properties of calcined carbon with 0–10 wt.% nano-SiC additions are summarized in Table 1.

3.3.1. Density and porosity

As shown in Table 1, the density of calcined carbon from pure GMCMBs was 1.73 g/cm^3. When doping with 3, 5, 10 wt.% nano-SiC, the density of GMCMBs–SiC samples increased remarkably and the maximum value arrived at 1.84 g/cm^3. However, the density of SMCMBs–SiC samples was lower than that of the GMCMBs–SiC samples, especially the minimum of 1.62 g/cm^3 was obtained for the SMCMB–10SiC sample.

The change tendency of open porosity was opposite to that of the bulk density. The open porosities of calcined carbon from the GMCMBs–SiC system were lower than those of the SMCMBs–SiC system accordingly, except that the two values were somewhat similar when with 3 wt.% dopant. The GMCMB–5SiC sample held the lowest open porosity of 8.7%, corresponding to the highest density value. Fig. 5 shows the SEM photographs of polished surfaces of calcined SMCMBs without dopant and with 5 wt.% nano-SiC. There were a lot of pores in the SMCMBs–0SiC sample (Fig. 5a). When doping with 5 wt.% nano-SiC, the calcined carbon became dense and few pores can be seen (Fig. 5b). Furthermore, layered carbon structure can be also seen clearly (Fig. 5c), indicating that the layered structure of MCMBs was retained after milling and the doping of nano-SiC contributed to the graphitization of calcined carbon.

In addition, although there were some large pores on the surface of the green body (Fig. 2), all the samples became dense after sintering. Moreover, no cracks were discovered in all the sintered samples during polishing, indicating that the catalytic effect of nano-SiC can promote particle rearrangement and structure improvement during sintering.

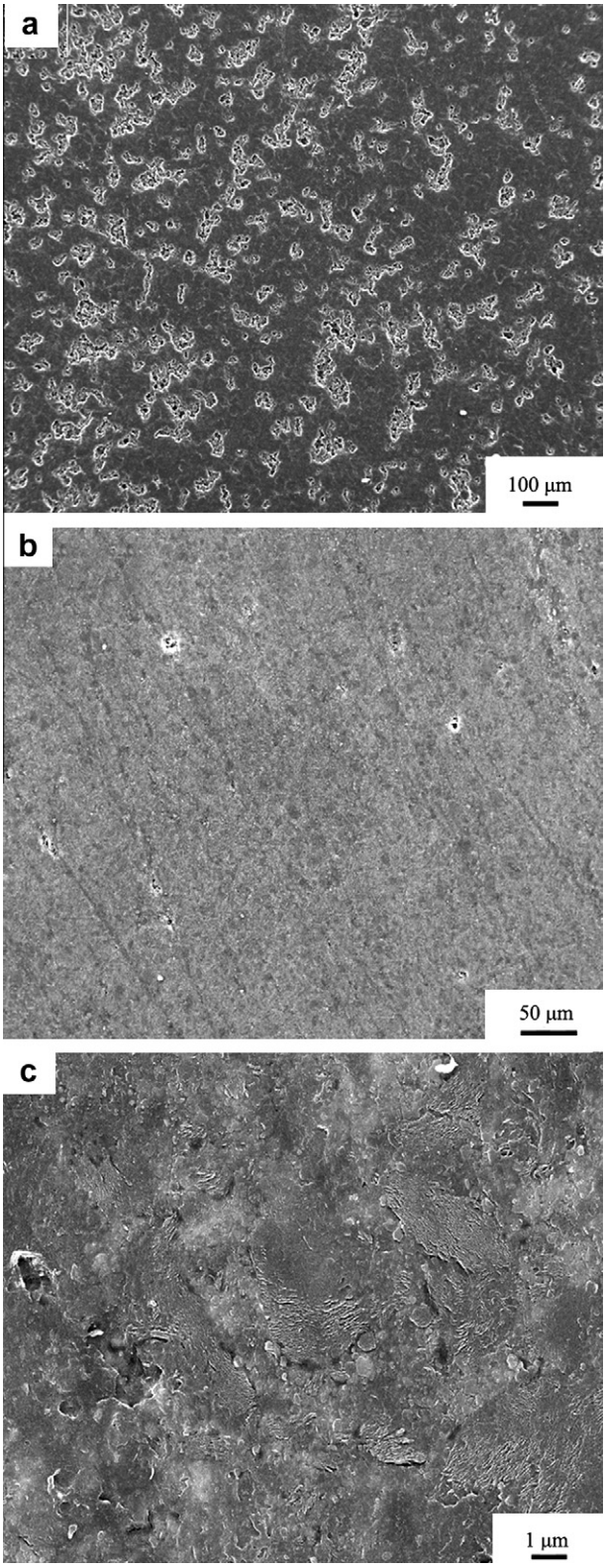

Fig. 5. SEM photographs of polished surfaces of the calcined SMCMBs: (a) 0SiC, (b) and (c) 5SiC.

3.3.2. Electrical resistivity

The lowest values of electrical resistivity, 28 and 29 μΩ m, were obtained in the calcined GMCMBs–5SiC and SMCMBs–5SiC samples, respectively. For carbon materials, the electric conductivity of all grades is dominated by π electron transmission along the carbon basal planes of hexagons, so that the crystallite interlayer spacing (d_{002}) and porosity are the main factors affecting the electrical resistivity. The lower the d_{002} and porosity values are, the more easily the π electron transmits through the materials, resulting in higher electric conductivity. The crystallite interlayer spac-

ing of calcined SMCMBs with different nano-SiC concentration are listed in Table 2. The d_{002} value decreased from 0.3490 nm to 0.3475 nm with increasing the nano-SiC concentration from 0 to 10 wt.%. As a result, the SMCMBs–5SiC sample held the lowest electric resistivity in the SMCMBs–SiC system based on the values of d_{002} and total porosity (the lowest porosity was 11.5% when doping with 5 wt.%), as shown in Table 1.

3.3.3. Bending strength

Bending strength of bulk materials is one of important characterizations for mechanical properties and it is mainly influenced by grain size, porosity and other defects [18]. The relationship between fracture strength σ_f and the grain size d is expressed by the equation:

Table 2
Crystallite interlayer spacing of calcined SMCMBs with different nano-SiC concentrations.

Samples	d_{002}(nm)
SMCMBs–0SiC	0.3490
SMCMBs–3SiC	0.3486
SMCMBs–5SiC	0.3484
SMCMBs–10SiC	0.3475

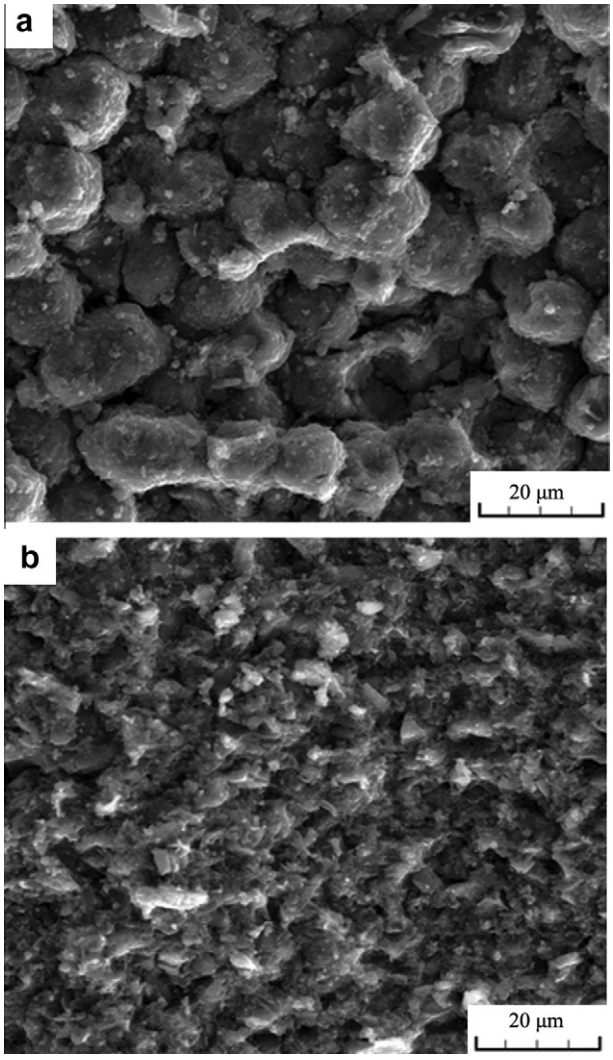

Fig. 6. SEM photographs of cross-sections of the calcined SMCMBs: (a) 0SiC and (b) 5SiC.

$$\sigma_f = \sigma_0 + Kd^{-1/2} \quad (3)$$

where σ_0 and K are two constants related with materials.

The effect of porosity P on fracture strength σ_f is expressed by

$$\sigma_f = \sigma_0 \exp(-nP) \quad (4)$$

where σ_0 and n are also two constants related with materials. So, the fracture strength can be improved by reducing grain size, porosity or defects, according to the Eqs. (3) and (4).

The bending strength values of calcined carbon without dopant were about 60 MPa for the two systems, and a suitable addition of nano-SiC can obviously improve the strength (Table 1). The high bending strengths of 122 and 98 MPa were obtained for the GMCMBs–5SiC and SMCMBs–5SiC samples, respectively, which possessed the smallest total porosities of 9.5% and 11.5%, correspondingly (Table 1). For pure MCMBs, the size distribution was usually narrow [2,4], and some gaps between spheres could be easily introduced into bulk sample, bringing about a bad effect on properties. Fig. 6 shows the cross-sectioned microstructures of the calcined SMCMBs–0SiC and SMCMBs–5SiC samples. It is obviously that many gaps between spheres existed in the SMCMBs–0SiC sample (Fig. 6a). However, there were no clear gaps existed in the calcined carbon when doping with 5 wt.% nano-SiC (Fig. 6b), because the spherical MCMBs particles became the smaller ones after milling (Fig. 1). This revealed that the milling process can reduce the particles size of the MCMBs and hence reduce or eliminate the gaps in the calcined MCMBs/nano-SiC materials to a certain extent, resulting in the improvement of the bending strength. In addition, the catalytic effect of nano-SiC on promotion of particle rearrangement and structure improvement contributed to obtain a homogeneous fine-dense texture, and can further improve the mechanical properties.

4. Conclusions

Calcined carbon materials derived from green or pre-oxidative mesocarbon microbeads (MCMBs) doped with 0–10 wt.% nano-SiC powder was prepared. The related sintering behaviors, physical and mechanical properties were investigated. Compared to the green calcined samples, the sintering shrinkage and density increment after pre-oxidation decreased accordingly, due to the relatively low content of viscous phase in samples before sintering. The two parameter (sintering shrinkage and density increment) values of all the calcined samples doped with 5 wt.% nano-SiC are higher than those with 3 wt.% and 10 wt.% dopants accordingly.

Physical and mechanical properties improved remarkably after doping a certain amount of nano-SiC powder. The highest bulk density and bending strength, as well as the lowest total porosity and bending strength were obtained with values of 1.84 g/cm^3, 122 MPa, 9.5% and 28 μΩ m, respectively, when doping 5 wt.% nano-SiC in the green MCMBs. Ball-milling contributed to the reduction of particle sizes of the MCMBs–SiC mixtures and hence reduced or eliminated the gaps between particles in the calcined composite. The catalytic effect of nano-SiC can promote particle rearrangement and structure improvement during sintering.

Acknowledgements

This work was funded by National Natural Science Foundation of China (Nos. 50972117 and 50802073).

References

[1] I. Mochida, R. Fujiura, T. Kojima, H. Sakamoto, T. Yoshimura, Carbon 33 (1995) 265–274.
[2] Y.G. Wang, Y. Korai, I. Mochida, Carbon 37 (1999) 1049–1057.
[3] I. Mochida, Y. Korai, C.H. Ku, F. Watanabe, Y. Sakai, Carbon 38 (2000) 305–308.

[4] Y.Z. Song, G.T. Zhai, J.R. Song, G.S. Li, J.L. Shi, Q.G. Guo, Carbon 42 (2004) 1427–1433.
[5] G. Bhatia, R.K. Aggarwal, N. Punjabi, O.P. Bahl, J. Mater. Sci. 32 (1997) 135–139.
[6] J. Schmidt, K.D. Moergenthaler, K.P. Brehler, J. Arndt, Carbon 36 (1998) 1079–1084.
[7] M.H. Chen, G.T. Wu, G.M. Zhu, J. Solid State Electrochem. 6 (2002) 420–427.
[8] C. García–Rosales, I. López–Galilea, N. Ordás, C. Adelhelm, M. Balden, G. Pintsuk, J. Nucl. Mater. 386–388 (2009) 801–804.
[9] C. Norfolk, A. Mukasyan, D. Hayes, P. McGinn, A. Varma, Carbon 42 (2004) 11–19.
[10] C. Norfolk, A. Kaufmann, A. Mukasyan, A. Varma, Carbon 44 (2006) 301–306.
[11] R. Fujiura, T. Kojima, M. Komatsu, I. Mochida, Carbon 33 (1995) 1061–1068.
[12] C.J. Zhou, P.J. McGinn, Carbon 44 (2006) 1673–1681.
[13] C. García–Rosales, N. Ordás, E. Oyarzabal, J. Echeberria, M. Balden, S. Lindig, J. Nucl. Mater. 307–311 (2002) 1282–1288.
[14] I. López-Galilea, N. Ordás, C. García-Rosales, S. Lindig, J. Nucl. Mater. 386–388 (2009) 805–808.
[15] X.B. Hu, G. Cheng, B.Y. Zhao, H.M. Wang, K.A. Hu, Carbon 42 (2004) 381–386.
[16] Z.J. Liu, Q.G. Guo, J.R. Song, L. Liu, Carbon 45 (2007) 146–151.
[17] C. Norfolk, A. Mukasyan, D. Hayes, P. McGinn, A. Varma, Carbon 44 (2006) 293–300.
[18] Z.D. Guan, Z.T. Zhang, J.S. Jiao, Physical Properties of Inorganic Materials, China, 1992.